Journal of Bioenergetics and Biomembranes, Vol. 32, No. 5, 2000

The α/β Interfaces of $\alpha_1\beta_1$, $\alpha_3\beta_3$, and F_1: Domain Motions and Elastic Energy Stored during γ Rotation[1]

Yasuo Kagawa,[2,3] Toshiro Hamamoto,[2] and Hitoshi Endo[2]

ATP synthase (F_oF_1) consists of F_1 (ATP-driven motor) and F_o (H^+-driven motor). F_1 is a complex of $\alpha_3\beta_3\gamma\delta\varepsilon$ subunits, and γ is the rotating cam in $\alpha_3\beta_3$. Thermophilic F_1 (TF_1) is exceptional in that it can be crystallized as a β monomer and an $\alpha_3\beta_3$ oligomer, and it is sufficiently stable to allow $\alpha\beta$ refolding and reassembly of hybrid complexes containing 1, 2, and 3 modified α or β. The nucleotide-dependent open–close conversion of conformation is an inherent property of an isolated β and energy and signals are transferred through α/β interfaces. The catalytic and noncatalytic interfaces of both mitochondrial F_1 (MF_1) and TF_1 were analyzed by an atom search within the limits of 0.40 nm across the $\alpha\beta$ interfaces. Seven (plus thermophilic loop in TF_1) contact areas are located at both the catalytic and noncatalytic interfaces on the open β form. The number of contact areas on closed β increased to 11 and 9, respectively, in the catalytic and noncatalytic interfaces. The interfaces in the barrel domain are immobile. The torsional elastic strain applied through the mobile areas is concentrated in hinge residues and the P-loop in β. The notion of elastic energy in F_oF_1 has been revised. X-ray crystallography of F_1 is a static snap shot of one state and the elastic hypotheses are still inconsistent with the structure, dyamics, and kinetics of F_oF_1. The domain motion and elastic energy in F_oF_1 will be elucidated by time-resolved crystallography.

KEY WORDS: ATP synthase; F_1; elastic energy; domain motion; hinge; F_oF_1; α/β interface; rotation thermophilic; X-ray crystallography.

In review, published in this journal (Kagawa and Hamamoto, 1996), we supported the rotational hypothesis of ATP synthase (F_oF_1) (Boyer, 1997 and references therein) and predicted that the torque of the rotation is 42 pN·nm via elastic energy transiently stored in F_oF_1 (Kagawa, 1999). In that issue, the Editor recommended that methodologies be developed that will allow subunit movements to be monitored as a function of time and captured directly on film (Pedersen, 1996). In fact, the intramolecular rotation of γ in the fixed $\alpha_3\beta_3\gamma$ of thermophilic F_1 (TF_1) has been visualized using single-molecule imaging (Noji *et al.*, 1997; Yasuda *et al.*, 1998; Kinoshita, 1999), and the rotation theory was established. The unsolved question is the analog–digital conversion of energy in F_oF_1. The electrochemical energy of the H^+ current (Mitchell, 1979) through F_o in liposomes (Kagawa and Racker, 1971) and a planar bilayer (Hirata *et al.*, 1986), and the mechanical energy of the rotation are analog quantities. The number of ATP molecules released from

[1] Key to abbreviations: F_oF_1, ATP synthase; F_1, catalytic portion of F_oF_1; F_o, ion-conducting portion of F_oF_1; MF_1, TF_1, and EF_1, F_1 from mitochondria, thermophilic bacillus PS3, and *E. coli*, respectively; $\alpha_3\beta_3\gamma\delta\varepsilon$, subunits of F_1; DCCD, dicyclohexylcarbodiimide; DELSEED, -Asp-Glu-Leu- Ser-Glu-Glu-Asp- sequence in the N-terminal region of β (in TF_1, it is DELSDED); loop AB, loop connecting the flanking secondary structures A and B; P-loop, -Gly-X-X-X-X-Gly-Lys-Thr-sequence of both the α and β subunit of F_1; 2,8-diN3-ATP, 2,8-diazido-ATP; SL-ATP, spin-label ATP, AMP–PNP, 5′-adenylyl-imido diphosphate; Bz-ADP, 3′-*O*-(4-benzoyl) benzoyl-ATDP; OSCP, oligomycin-sensitivity conferring protein; OOO, α_3(open β)$_3$ form; OOC, α_3(open β)$_2$ (closed β) form; OCC, α_3(open β) (closed β)$_2$ form; CCC, α_3(closed β)$_3$ form. An example of residue nomenclature: TβE190, Glu190 (E190) residue of the $TF_1\beta$ subunit. I–XI, area of contact in the α/β interfaces.

[2] Department of Biochemistry, Jichi Medical School, Minamikawachi, Tochigi, 329-0498, Graduate School, Women's University of Nutrition, Sakado, Saitama 350-0288, Japan.

[3] To whom all correspondence should be addressed: e-mail: ykagawa @jichi.ac.jp or kagawa@sak.eiyo.ac.jp

0145-479X/00/1000-0471$18.00/0

the catalytic site is a digital quantity. Despite the analog–digital conversion, F_oF_1 shows a fixed stoichiometry and nearly 100% energy efficiency (Yasuda *et al.*, 1998). To convert the $\pi/5$ step rotation of F_o into the $2\pi/3$ step rotation of F_1, we predicted elastic energy (Kagawa and Hamamoto, 1996). Since rotation occurs during the time lag that follows the hydrolysis of ATP, there must be transient elastic energy stored in F_oF_1 (Kagawa, 1999).

Recently, the elastic energy of F_oF_1 has been calculated on the hypothetical "four-step stress accumulation" (Cherepanov *et al.*, 1999) or "binding zipper" (Oster and Wang, 2000). However, the following experimental data are inconsistent with their calculation.

1. It is based on the graphical rotation (http://nature.berkeley.edu/-hongwang/ATP-synthase) of X-ray crystallography of F_1 (Abrahams *et al.*, 1994). However, it is a static snap shot of one state during rotation and ATPase is inactive in that crystallizing condition (high Mg^{2+}, ADP, and AMP–PNP).

2. The reported number of *c* subunits in F_o is 12 (Jones *et al.*, 1998), whereas the X-ray crystallography indicates that this number is 10 (Stock *et al.*, 1999). Thus, F_o is rotated by the $\pi/5$ step, not the $2\pi/3$ step rotation of F_1 that is used for their calculation. The single-molecule analysis of rotating F_oF_1 (Sambongi *et al.*, 1999) was refuted because of defective F_o (Tsunoda *et al.*, 2000).

3. In contrast to the X-ray crystallography (Abrahams *et al.*, 1994), all sites are fully occupied by Mg–nucleotides during the steady state (Weber and Senior, 2000). The fully occupied F_1 was also suggested by X-ray crystallography (Bianchet *et al.*, 1998).

4. The calculation is based on the unisite catalysis at the ATP concentration of 1 mM (Fig. 4 of Ref. Oster and Wang, 2000). However, the F_1 rotation is observed at the bi- and trisite catalysis (Yasuda *et al.*, 1998).

5. TF_1 is harder than mesophilic F_1s. The strain–stress relationship should be different, yet the synthesis/hydrolysis of ATP is identical (Kagawa and Hamamoto, 1997).

6. Athough γ is a putative torsional spring according to Cherepanov *et al.* (1999), it is not limited to γ but is distributed among residues including hinge-controlling interfaces of subunits.

7. Tritium exchange (Noji *et al.*, 1996) and IR (Ohta *et al.*, 1980) failed to detect "the zippering of H bonds" (Oster and Wang, 2000) in both TF_1 and γ during ATP hydrolysis. The long-reaching electrostatic force is more important than the H bond (0.3 nm, directional) and van der Waals forces (short range) in elastic domain displacement.

Such elastic strain must be transferred through the subunit interfaces into a heterogeneous solid composed of the α-helices, β sheets, and loops. The molecular structure of the ATP-binding site located at the α/β interface has been visualized by X-ray crystallography (Abrahams *et al.*, 1994; Shirakihara *et al.*, 1997; Bianchet *et al.*, 1998). F_1s from thermophilic bacteria (T) (Kagawa *et al.*, 1986), mitochondria (M)(Kagawa *et al.*, 1997), and *E. coli* (E) (Futai *et al.*, 1989), are called TF_1, MF_1, and EF_1, respectively, and have various advantages in the structure study.

This review analyzes the molecular dynamics of the α/β-subunit interfaces and hinges based upon data obtained by Yoshida's group and ours. Contact residue pairs within 0.40 nm across the α/β interfaces in $\alpha_3\beta_3$ complex (Shirakihara *et al.*, 1997) and MF_1 (Abrahams *et al.*, 1994) were computed using the CCP4 Suite: Program Contact. Detailed structures of Tβ can be viewed via the internet at NCBI MEDLINE PubMed MMDB Id:7378 PDB Id:1SKY. Detailed mutational studies on EF_1 have been performed (Weber and Senior, 2000; Futai *et al.*, 1989) and the proposed imaginary roles of the residues will be examined in the light of physical data on TF_1. Open and closed conformations are known for β and the theoretical treatment of the domain motions of 24 proteins with two conformers has been reported (Hayward, 1999).

STATOR AND ROTOR IN F_oF_1

Components of F_o and F_1 (Fig. 1)

We prepared and reconstituted MF_oF_1 from MF_o and MF_1 (Kagawa and Racker, 1966a) and then assembled TF_1 from refolded subunits (Yoshida *et al.*, 1975). The subunit compositions of F_1 and prokaryotic F_o are $\alpha_3\beta_3\gamma\delta\varepsilon$ and ab_2c_{10}, respectively. The $\gamma\varepsilon$ subunits of F_1 rotate in the cavity of $\alpha_3\beta_3$ fixed by δb_2 to F_o-*a* subunit. F_1 is about 370 kDa, and the sequence of α (55 kDa), β (52 kDa), and γ (30–32 kDa) subunits are homologous among F_1s of all species. The isolated α and β both have AT(D)P binding sites. In MF_oF_1, OSCP, and δ corresponds to δ and ε, respectively, of prokaryotic F_1. MF_o contains, in addition to the common *a*, *b*, and *c*, specific subunits *d*, *e*, *f*, *g*, F_6, A6L, and OSCP (Collinson *et al.*, 1996).

Single-Stalk F_oF_1 and Rotation

F_oF_1 was identified as a sphere (diameter 12×10 nm, $\alpha_3\beta_3$) connected by two stalks (central and peripheral) to a basal piece (Wilkens and Capaldi, 1998). The central stalk contains $\gamma\varepsilon$, and the peripheral stalk, δ–F_o-*b* (Fig. 1, lower right). The $\gamma\varepsilon$ is the eccentric shaft

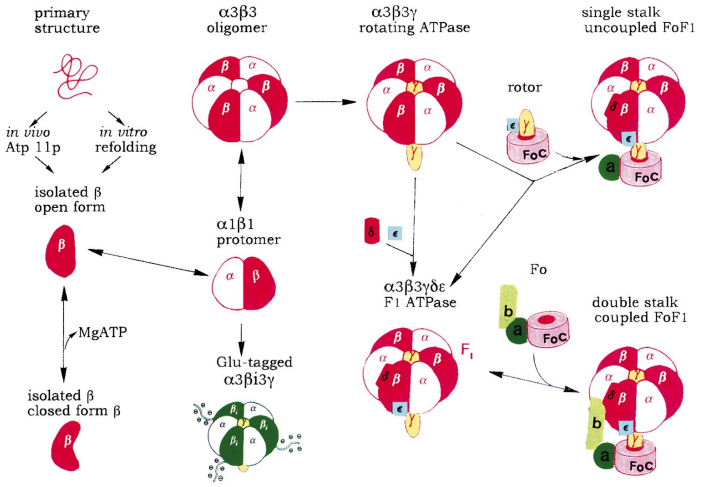

Fig. 1. Refolding and assembly of subunits of thermophilic F_1. The nomenclature of subunits is described in the text. F_1 subunits are α, β, γ, δ, and ε. F_o subunits are *a*, *b*, and *c*. Details have been reported (Kagawa, 1999).

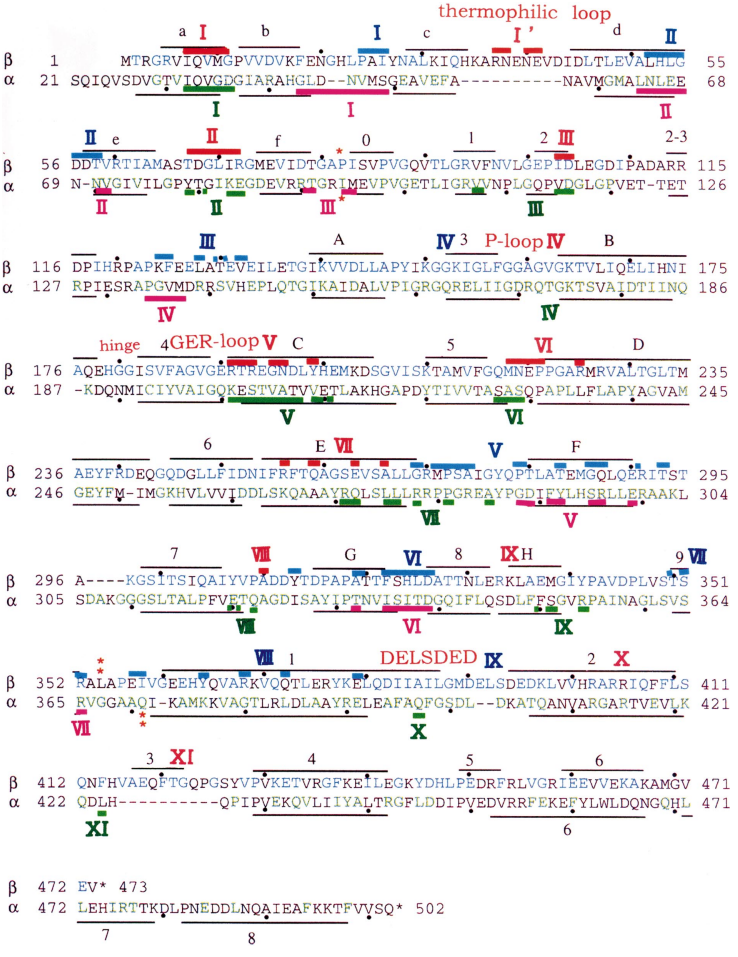

Fig. 2. Catalytic and noncatalytic $\alpha\beta$ interfaces located on aligned amino acid sequences and secondary structure elements of α and β subunits in TF_1. Solid black lines indicate folds and these are classified into α-helices (A–H, 1–8) and β-sheets (a–f, 0–8). Folds of both subunits are similar and labels are thus provided only for the β subunit, except for the three C-terminal α-helices in the α subunit. Dots indicate every tenth residue. I–XI: areas of $\alpha\beta$ contact. Red, catalytic contact areas of β; Pink, catalytic contact areas of α blue, noncatalytic contact areas of β; green, noncatalytic contact areas of α. Colored bars indicates contact residues in $T\beta_E$. Sequences are divided by red asterisks to indicate the three domains. Original sequence data (Kagawa *et al.*, 1986) are aligned as described (Kagawa, 1999).

and δ–F_o-*b* is the part of stator that fixes $\alpha_3\beta_3$ to F_o-*a*. In this double stalk F_oF_1 torque of the $\gamma\varepsilon$-F_o-*c* rotor induces a conformational change of $\alpha\beta$ (Fig. 1).

The single molecule analysis of rotating F_oF_1 (Sambongi *et al.*, 1999) is controversial because of defective F_o (Tsunoda *et al.*, 2000). The earliest electron micrograph of F_oF_1 showed only a central stalk (Kagawa and Racker, 1966b). This single stalk F_oF_1 was reconstituted from both ^{3}H-acetyl-F_1 and urea–cholate-treated F_o devoid of the peripheral stalk (Kagawa and Racker, 1966b) (Fig. 1, upper right). This single-stalk F_oF_1 restored coupling activity by adding OSCP and other extracted crude factors (Kagawa and Racker, 1971) by forming the stator. In fact, X-ray crystallography of detergent-treated F_oF_1 revealed a single stalk (Stock *et al.*, 1999), because both F_o-*a* and F_o-*b* were lost. The resulting single-stalk F_oF_1 shows the rotation of F_o that reflects the $2\pi/3$ steps of γ, not the $\pi/5$ steps of F_o-*c* subunits (Tsunoda *et al.*, 2000).

PRIMARY STRUCTURE OF THE α AND β SUBUNITS

We sequenced TF_oF_1 (Kagawa *et al.*, 1986) and human MF_1 (Ohta and Kagawa, 1986). The numbers of amino acid residues in the aligned sequences in Tα and Tβ are shown in Fig. 2. With respect to nomenclature for the amino acid residues in the subunits α, β, γ, etc., of TF_1, MF_1, and EF_1, "TβK35," for example, means that a lysine (K) residue is located at No 35 in the β subunit of TF_1 (Tβ). The equivalent residues in different F_1s are expressed as TβK164 (=MβK162, EβK155). A mutation is abbreviated as "TβK164I," which means "the residue K164 of Tβ is changed into I164." The primary structures of the α and β subunits from TF_1 (Tα and Tβ) and MF_1 (Mα and Mβ) are homologous with 59% sequence identity between Tα/Mα and 68% between Tβ/Mβ. Conserved residues (green and blue letters in Fig. 2) among TF_1, MF_1, and EF_1 are closely related to catalytic and regulatory functions. Species-specific residues (black letters in Fig. 2) may have phylogenic and ontogenic meaning. A detailed phylogenic tree of F_1 was drawn using the protein database. According to our studies using transgenic mice, γ-subunit isoforms are produced by splicing during ontogenesis (Ichida *et al.*, 2000; Kagawa *et al.*, 1997).

DOMAINS OF α AND β, AND OPEN–CLOSE MOVEMENTS

Three Domains of the α and β Subunits

The tertiary structure of Tα, Tβ (Shirakihara *et al.*, 1997), Mα, and Mβ (Abrahams *et al.*, 1994) consists of three domains (Fig. 3). These are an N-terminal β-barrel (Tα21–94, Tβ1–82), a central nucleotide-binding region (Tα 95–371, Tβ83–354), and a C-terminal α-helical bundle (Tα375–502, Tβ355–473) (Figs. 2 and 3). The barrel domain contains six β sheets (a–f) arranged like an IgCI fold (pairs of a–b, c–f, and d–e strands) and the barrel structure is found in SH3 (*src* homology 3). The nucleotide-binding domain consists of a nine-stranded β sheet (1–9) surrounded by eight α helices (A–H) and a small additional antiparallel β sheet (0 and 2.1) (Fig. 2) structures, which are similar to the nucleotide-binding domains of G proteins. The C-terminal domain consists of six α-helices in Mα and Tα(helices 1, 2, 4, 6–8), and in Mβ and Tβ (helices 1–6) (Fig. 2). Thus, the largest difference between α and β is in the C-terminal region. The α–helical bundle is also found in helical cytokines. The loops are located at the central cavity and peripheral surface and play important roles.

THE OPEN- (β_E) AND CLOSED FORM (β_D, β_T) OF β SUBUNIT

The nucleotide-free crystal of $\alpha_3\beta_3$ (Shirakihara *et al.*, 1997) shows strict threefold symmetry. In contrast, because of the presence of one copy of $\gamma\delta\varepsilon$ and $\alpha_3\beta_3$ per F_1 molecule, the threefold symmetry in the crystallography of F_1 is an approximation and γ is disordered (Bianchet *et al.*, 1998). Bovine heart MF_1 crystallized in D_2O containing AMP–PNP, ADP, Mg^{2+}, azide, and Tris shows three different states of β (Abrahams *et al.*, 1994) that have ADP (β_D), AMP–PNP (β_T), and no nucleotide (β_E), respectively. The original rotational theory assumed the loose-, tight-, and open-β conformations (Boyer, 1997). The β_T and β_D have very similar conformations, but β_E is quite different (Abrahams *et al.*, 1994), and both β_D and β_T are classified as closed forms (C), while β_E has the open form (O). Tβ_E in $\alpha_3\beta_3$ superimposes well on the whole Mβ_E. Thus, $\alpha_3\beta_3$ is OOO type (Shirakihara *et al.*, 1997) and bovine MF_1 crystal is CCO type (Abrahams *et al.*, 1994). However, rat liver MF_1 crystallized in H_2O containing ATP and P_i (without Mg^{2+}) has threefold symmetry and the structure seems to be of the CCC type (Bianchet *et al.*, 1998), because all Mβs have ADP and two may have P_i. However, formation of the CCC type by adding ADP to $\alpha_3\beta_3$ causes its dissociation into $\alpha_1\beta_1$ (Sato *et al.*, 1995; Kagawa *et al.*, 1992), because two β_Ds collide at TβI396 (Fig. 3, left bottom I in red circle). In fact, the β-β is cross linked at these residues and the CCC type was refuted (Tsunoda *et al.*, 1999).

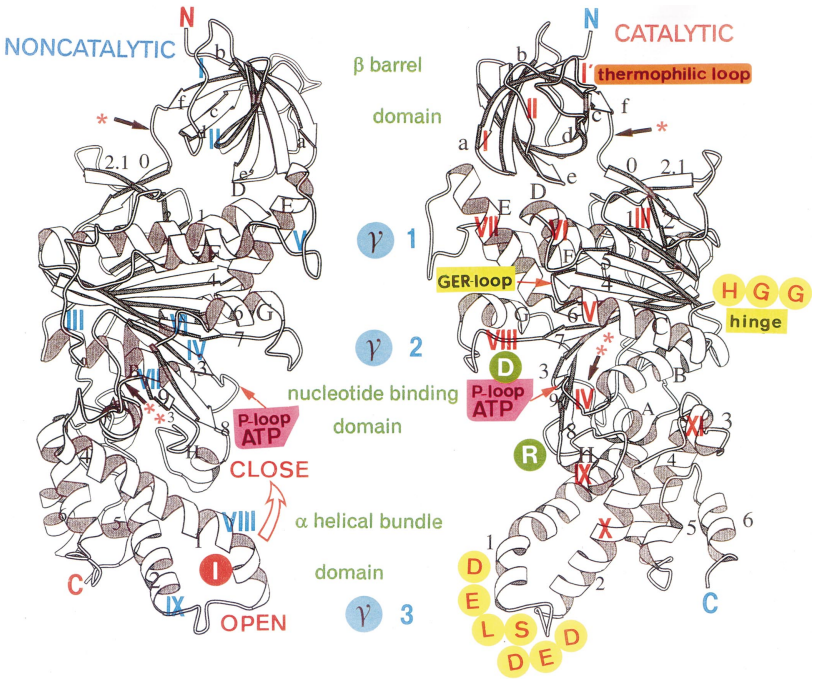

Fig. 3. Three-dimensional structures of Tβ_E. Threefold axis is vertical, so that views are toward the α/β subunit interfaces. Left, noncatalytic interface (blue I–IX indicates contact areas). Right, catalytic interface (red I–XI indicates contact areas). Green letters, domain names and the border of domains are marked by red asterisks. D and R in green circles are TβD331 and TβR333, respectively, at the entrance to the crevice of the P-loop. I in red circle is TβI386 of $\beta\beta$ contact. H and Gs in yellow circles are the hinge residues. (Modified from Shirakihara *et al*., 1997.)

THE CATALYTIC AND NONCATALYTIC $\alpha\beta$ INTERFACES

The α/β Interfaces

The α and β contact each other via catalytic and noncatalytic interfaces, and these are expressed as primary structures in Fig. 2 for Tα and Tβ, and Table I for Mβ. Except for the thermophilic loop, homological contact areas (I–XI) are located in both and β and α at catalytic (red and pink bars in Fig. 2), and noncatalytic (blue and green bars in Fig. 2) interfaces. These areas in Tβ are shown in Fig. 3.

The barrel domain harbors the universal contact areas I and II (Table I and Fig. 2). The common electrostatic bond in II is TβR72–TαE67 (=MβR71–MαE67). At the catalytic nucleotide-binding domain, areas III, V, VI, VII, and VIII are universally detected (Table I). However in Tβ_E, the P-loop contact area IV is latent, in contrast to that area in Tα_E (Fig. 2), Mβ_T, and Mβ_D (Table I). MαR373 interacts with oxygens of β- and γ- P of ATP bound at IV. In V, the common electrostatic bonds are TβR193–TαD339 and MβR191–MαD347. In VI and VII of β_T and β_D, MαF299–MβM222 and MαS344–MβR260, respectively, interact. However, we identified no direct contact in the α-helical bundle domain in Tβ_E of OOO type F_1. In the catalytic α/β interface of Mβ_E, the contact areas (17.6 nm^2) are homologous to those of Tβ (Table I). The areas of Mβ_D (30.3 nm^2) and Mβ_T (22.0 nm^2) are increased to 11 and 10, respectively (Table I). This is caused by the $\pi/6$ upward motion of the C-terminal domains.

The seven main contact areas of the noncatalytic α/β interface of Mβ_E in are summarized in Table I (areas I–VII). In Mβ_E, the contact areas of the noncatalytic α/β interface are homologous to those of Tβ_E (Fig. 2). The noncatalytic site of α accepts MβD359 (VII) that interacts with the ribose of AMP–PNP. In the closed form of Mβ, these areas are changed in Mβ_D (9) and Mβ_T (7) (Table I, bottom).

The catalytic interface of α has five contact areas between β_E, but the number of these areas increased to 8 and 7 between β_D and β_T, respectively. In the closed Mβ, αR373 interacts with, in addition to AT(D)P, both V (βR189 bR191) and IV (βG159), because α-helices B and C move closer. However, the noncatalytic interface of α has seven contact areas between β_E, β_D, and β_T. The target α areas of I–XI of β are shown in Table I. Because

Table I. Catalytic and Noncatalytic $\alpha\beta$ Interfaces of MF_1 β Subunit

	Catalytic $\alpha\beta$ interface (I–XI: contact areas and their location) The major charged groups for intersubunit interactions: D, E, R, H, and K					
Ligand[a]	I Sheet *a*	II Loop *e*–*f*	III Sheet 1, 2	IV P-loop	V Helix C	VI Sheet 5, helix D
	14 18	64 66 68 71	94 102 104	158 159	189 192 194 197	219 222 226 229
E	VAVIG	DGT–GLVR	I—IDE	——	RTRE–ND–Y	Y—MNEP—R
D	VAVI	D–TEGLVR	ID	AG	RTR—ND–Y	Y—MNEPP—R
T	AVI	D–TEGLVR	I—IDE	AG	RTR—ND–Y	Y—MNEP—R
target α	sheet *d*	sheet *c*, loop A	loop A	helix G	helices F, G	loop A, helix F

	Catalytic $\alpha\beta$ interface (I–XI: contact areas and their location)				
	VII Helix E, γ-Loop F	VIII γ-Loop G	IX α-Helix H	X α-Helix 2	XI α-Helix 3, 5
	260 263 267 273 281	311 314 319	337 341 345	388 404 412	423 424 453 455 458
E	–E–AL–G–	——A——	——	——	——
D	R–Q–E–A——V–Y	Y–AD–D	R—ELG-Y	I-V-R-R	VFTGH-P–QY
T	R–Q–E–A–P–V	Y–ADD-D	R——	——	VF——Q
target α	loop F, helix F, γ	helix G, γ	loop G, ATP-Y	loop 2, γ	loop 1-helix 1

	Noncatalytic $\alpha\beta$ interface (I–IX: contact areas and their location)				
	I Loop *bc*	II Sheet *d*	III Loop *d*–*A*	IV Sheet 3	V γ-Loop F, helix F
	29 31 32	51 54 56	119 124 128 130	151	273 275 278 283 287 290 294
E	L-PI	QHLGES	EAPEFV-M-VEQ	K	GRIPSA-PT—T-G———E
D	L-PI	QHLGES	EAPEFV-M-V-Q	K	GRI-SA-PT—T-GT—E
T	L—I	QHLGES	EAPEFV-MSV-Q	——	GRIPSA-PT-AT-GT—E
target α	loop *f*	sheet *a* loop *f*	sheet *f*, helix C	loop C	helix F, loop F

	Noncatalytic $\alpha\beta$ interface (I–IX: contact areas and their location)			
	VI γ-Loop, helix G	VII Sheet 9	VIII Helix 1	IX DELSEED-loop
	317 316 330	351 355 356 359	368 372 375 380 383 387	395 397 400
E	-TA-FAH-D	——R——D	——	——
D	LT—FAHLD	LDSTR———D	———QK—QD-SL—I	ELS———D
T	-T—FAHLD	LD–TR———D	Y-R-QK—QD-S—	——
target α	loop B, sheet 4	P-loop, helix C	helix H, loop-helix 2	loop-helix 2

[a] Ligands on the β subunits: E, no ligand; D, ADP; T, AMP–PNP.

of the high homology between TF_1 and MF_1, the total numbers of atoms in the areas of catalytic interface of $T\beta_E$ and $M\beta_E$ were 91 and 93, respectively, if the TF_1-specific area of the thermophilic loop (11 atoms, I′ in Fig. 2) is removed. Those of the noncatalytic interface of $T\beta_E$ and $M\beta_E$ were 112 and 114, respectively. In contrast, the atom numbers (in parentheses) in the contact area were significantly increased in the closed forms: catalytic interface of $M\beta_D$ (176), $M\beta_T$ (131), and noncatalytic interface of $M\beta_D$ (141) and $M\beta_T$ (139), mainly at the lower half of the β.

The Immobile Areas for the Stator

The conformations of bovine Mα loaded with Mg-AMP–PNP (Abrahams *et al.*, 1994), rat liver Mα loaded with Mg-ATP (Bianchet *et al.*, 1998), and Tα without ligands (Shirakihara *et al.*, 1997) are equally open. The entire structure of the β-barrel domain of β_E superimposes well on that of β_D and β_T. Torsional strain in the β-barrel domain is low because of the distance from the β-γ contact points, slender mainchain connection (Fig. 3, red*), and firm binding through I, I′, and II. Thus, the β-barrel domain

of both α and β is immobile during the rotation. The stator may be connected to $\alpha_3\beta_3$ via δ attached to the barrel domain. In fact, OSCP was cross linked to the N-terminal of α (Xu *et al.*, 2000).

REFOLDING OF TF_1 SUBUNITS AND ELECTROSTATIC FORCE

In the stress-strain analysis, F_1 is not a uniform rubber ball, but the assembly of heterogeneous solid composed of α-helices, β sheets, and coils (Figs. 1 and 3). The forces to form the tertiary structure are propensity to form α-helices and β sheets, as well as external hydrophilicity and internal hydrophobicity of $\alpha\beta$. TF_1 was completely denatured and refolded (Yoshida *et al.*, 1975). During subunit refolding, the molecule assumes an expanded state called the "molten globule phase" in the order of milliseconds or less (Arai and Kuwajima, 2000). CD (Yoshida *et al.*, 1979), and D–H exchange (Ohta *et al.*, 1980) confirmed the refolding (Kagawa, 1999) (Fig. 1, upper left). In contrast to H bonding for secondary structures, etc., and van der Waals force for helical bundle fomation, etc., electrostatic force is long-reaching and plays an important role in domain movements (Hall and Pravitt, 1984). The primary structures of the TF_1 subunits contain refolding information which differs from those of other F_1. Stability (Argos *et al.*, 1979) and folding (Jaenicke and Boehm, 1998) of thermophilic proteins can be achieved by adding many small residue substitutions to the corresponding mesophilic proteins without significant change in backbone conformation. The rule for the general thermophilic protein (Argos *et al.*, 1979) was confirmed not only in TF_1 (Kagawa *et al.*, 1986) but also in hyperthermophilic V-ATPase (Shibui *et al.*, 1997), that is homologs of F_oF_1. The residues mainly contributing to the increased propensity of the secondary structure in Tβ are located near the barrel domain: sheets a (V6, I7, and Q8), c (K32 and H34), o (S84 and V85), and 1 (V95), and exceptionally in helix 1 (E361, Q365, K369, E375, and E379). The highly conserved α-helices (A–G and 2–6) contain residues with almost equal propensity in both MF_1 and TF_1.

The basic mechanism of the synthesis/hydrolysis of ATP is equal in TF_1 and mesophilic F_1s. Thus, the different stability is mainly limited in the immobile areas I, I′, and II (and helix I) not to areas III to XI.

ASSEMBLY MUTANTS

Site-directed mutagenesis produces many defective subunits (Futai *et al.*, 1989; Yagi *et al.*, 1999; Omote *et al.*, 1995). We located these mutant residues in X-ray crystallography of β_E, β_D, and β_T. If "assembly mutant residues" are strictly defined as those localized at the $\alpha\beta$-contact area to bind both subunits, very few are present: EαE299 (=MαE299, IV of α), EαS347 (=MαS344, V of α), EβE185 (=MβE192, area V of β), Eβ192 in helix C (V), and EβG214 (=MβG227, VI of β) of catalytic interface (Table I). Any denaturating mutation of mesophilic F_1 may be false "assembly mutation." An example of a real assembly mutant is TβY277F, which cannot assemble (Yagi *et al.*, 1999) at the noncatalytic interface V, and this tyrosine is conserved among species. Functionally, residues, such as EβE185, can be involved in cooperative catalysis (Omote *et al.*, 1995).

Other defective residues may indirectly affect conformations around the interfaces and the P-loop. For example, the EβG149C mutation in the P-loop is suppressed by EβS174F in strand 4, which is quite far from the P-loop (Futai and Omote, 1996). Furthermore, this defective coupling activity of the EβS174F mutant was suppressed by the second mutation, EαR296C, in helix F of α across the α/β interface. However, both mutations are not in direct contact. The fact that a mutation in β is suppressed by mutation in α, supports the notion of indirect $\alpha\beta$ interaction. If this kind of mutation causing indirect interactions is included in the catalytic mutation, the distinction between catalytic and assembly mutation becomes blurred.

In vivo Refolding and Assembly of F_1 Require Chaperones

The primary folding and assembly of peptides synthesized by mRNA translation require chaperones such as Atp11p protein in MF_1 (Wang and Ackerman, 2000). Atp11p binds to a region of the nucleotide-binding domain of Mβ located between MβG114 and MβL318 (IV–VIII) and assembled Mα. We cloned and characterized a hyperthermophilic chaperone to use as a tool for the refolding of subunits (Yoshida *et al.*, 1997). Since, *in vitro* refolding and reassembly are difficult in mesophilic F_1s, the *in vivo* assembly mutant may include mutants that are defective in the chaperone step.

NUCLEOTIDE-BINDING LOOPS

P-Loop in Area IV

The P-loop is found in many nucleotide-binding proteins, including α (noncatalytic site) and β (catalytic site) of F_1 (Abrahams *et al.*, 1994). The catalytic P-loop (GGAGVGKT; Tβ158–165, Fig. 3, pink) is located between sheet 3 and helix B. Most amide groups in the P-loop are involved in H bonding to the β-phosphate of AT(D)P. Thus, binding of ADP and ATP can equally form closed β. TβK164 (=MβK162) in the P-loop binds to the

γP of ATP, and TβK164I lost both nucleotide binding and catalysis abilities (Yohda *et al*., 1988). The true substrate bound at the P-loop is Δ, $\beta\gamma$-bidentate Mg, ATP complex (Senter *et al*., 1983). Mg^{2+} is required for the expression of catalytic site-binding cooperativity and high-affinity binding at catalytic site 1. The K_d values for sites 1, 2, and 3 are about $<$1nM, 1μM, and 100μM, respectively, in EF_1 (Weber and Senior, 2000). The hydroxyoxygen of TβT165 in the P-loop directly coordinates with Mg^{2+}. The ESR of both MF_1 and TF_1 spin labeled with 2-azido 2′, 3′-SL-ATP revealed the tightening role of Mg^{2+} (Burgard *et al*., 1994).

GER Loop in Area V

The nucleotide-binding domain of β accommodates the conserved TβE190 (=MβE188, EβE181) that may function as a general base to activate bound water by abstracting a proton. This residue is localized at loop 4C (=GER loop), and interacts with the γ-phosphate of ATP via a water molecule (Abrahams *et al*., 1994). The direct contact of helix C at V of the catalytic interface (Fig. 2) and the hinge motion of the C-terminal domain containing DELSEED in Mβ_E, rotates away from the core of the particle by almost $\pi/6$ (Abrahams *et al*., 1994). The resulting widening of the P-loop-TβE190 distance causes the release of Mg-ATP from the catalytic site.

Loop 7G in Area VIII

Loop 7G is located between sheet 7 and helix G of β. This loop is close to the P-loop in the closed form, but is distant from the P-loop in the open form. The conformational change is transferred to the P-loop via loop 7G, a putative switch region (Noji *et al*., 1996) located in VIII (Fig. 2) near TβD315, the closest point to the γ-axis (Fig. 3, γ2). G proteins and myosin (Sasaki *et al*., 1998) contain switch domains 1 and 2, and the latter is, to some extent, similar to VIII. As in G proteins, a nucleotide is bound around the α-helix B and the P-loop. The alanine scanning mutagenesis (D454A, G457A, F458A, and E549A) of myosin removed the motor function and G457A lost ATPase by blocking main-chain rotation because G457 corresponds to the γ-phosphate sensor glycine (G60 of Ras) in the G-protein (Sasaki *et al*., 1998).

PROPERTIES OF ISOLATED SUBUNITS

Monomeric Structure of the α and β Subunits

The diffraction pattern of mutant (Y341L) Tβ crystallized in the absence of Mg-nucleotide shows unit-cell dimensions of a = 232A, b = 66A, and c = 80A (Saika *et al*., 1994). The whole structure superimposes well on that of Mβ_E (Abrahams *et al*., 1994) and of Tβ_E (Shirakihara *et al*., 1997). This result indicates that the "open form" of β is not caused by the $\alpha\beta\gamma$ interaction (Fig. 1 lower left). The conformation of isolated Tα and Tβ was changed by adding Mg-AT(D)P as shown by IR (Ohta *et al*., 1980), NMR (Tozawa *et al*., 1995), CD, neutron scattering, and X-rays (Kagawa, 1999). In fact, the cross linking of TβD311 and TβR333 (Fig. 3, green D and R) fix the isolated β in a closed form, in which α-helix C (V) and α-helix B (IV) become parallel (Ren *et al*., 1999). The following X-ray data constitutes a personal communication from Prof. K. Miki. Because of the absence of the surrounding subunits, some contact areas, including the thermophilic loop (I′ in Fig. 2) of Tβ, are disordered. Among the contact areas at the catalytic sites in the Tβ shown in Fig. 2, the structures of areas I, II, III, VI, and VII are located very close to Mβ_E and Tβ_E. However, V in α-helix C (the closest helix to α) has no adjacent α-helices F and G in Tα, and part of α-helix C is disordered and expanded to the Tα side. Thus, both side-chain and main-chain folding of TβE190 and TβR191 in the GER loop of the isolated Tβ shifted from their positions in active $\alpha3\beta3$. The C-terminal regions are disordered, and the temperature factor (80Å^2) was much larger than that in the barrel- and nucleotide-binding domains. Among the noncatalytic contact areas, the structures of areas I and III have no interacting α-helices, and slide to the direction of missing α-helices. Except for the disordered VI, the other areas are almost identical to β_E in the oligomer.

Conformational dynamics of the isolated Tβ were monitored by TβH179 at the conical tunnel entrance and those of TβH200 were examined at catalytic V using [^{1}H]NMR. Binding of Mg-AMP–PNP significantly affected the chemical shift of both residues, indicating a ligand-induced conformational change (Tozawa *et al*., 1995). The 3,5-proton resonance of 12 tyrosine residues in Tβ revealed a Mg-ATP-dependent signal shift in Y199 at V, in Y307 at VIII, etc. (Yagi *et al*., 1999).

THE $\alpha_1\beta_1$ PROTOMER AND CATALYTIC INTERFACE

The assembly of $\alpha_1\beta_1$ protomer forms a catalytic interface (Kagawa *et al*., 1992). A sequence specific to TF_1 is located in the β barrel (Figs. 2 and 3, I′ Tβ36–42, or thermophilic loop). The thermophilic loop holds Tα and Tβ tightly at the catalytic interface by an H bond (βD40–αR90) and by van der Waals interactions (βN38–αS21 and βE41–αM48).

The nonactive catalytic site in the Tβ monomer is converted into the active catalytic site by a supply of residues in Tα (TαT338 in VI and TαR365 in VII). The

guanidium of MβR373 and the ε-ammonium of MβK162 interacts with the γ-P of Mg-ATP (Abrahams *et al*., 1994). TαR365 (=MαR373) may stabilize the terminal phosphate in a pentacoordinate transition state of the Δ,β,γ–bidentate Mg-ATP. However, the mutant of this residue still show unisite ATPase activity and EαR376 (=MαR373, TαR365) may be required for the promotion of the steady state (Le *et al*., 2000). MαR373 interacts with G159 (IV), R189 and R191 (V), and F424 (XI) in addition to the nucleotide (Table I). The kinetics of the ATPase of $\alpha_1\beta_1$ were typical Michaelis-Menten type (Saika and Yoshida, 1995), with only one K_m ATP value of 70μM, and a V_{max} value of 0.1 unit/mg, without cooperativity. The H bond between TβE201 (=MβE199) and TβT165 (=MβT163) stabilizes the open form, as shown by an experiment that used $\alpha_3\beta_3\gamma$ containing the mutant TβE201C (Ren and Allison, 2000). TβT165 interacts directly with Mg coordinated to ADP and Tβ becomes closed form.

THE $\alpha_3\beta_3$ OLIGOMER AND NONCATALYTIC INTERFACE

The noncatalytic, in addition to the catalytic interface, is now formed by the assembly of three $\alpha_1\beta_1$ into $\alpha_3\beta_3$ (Kagawa *et al*., 1992; Sato *et al*., 1995). The noncatalytic nucleotide-binding site is formed at the αP-loop with TβD326, TβR352, and TβY364 on the noncatalytic α/β interface. In contrast to $\alpha_1\beta_1$, the ATPase activity of $\alpha_3\beta_3$ is cooperative. Depending on the occupancy of the catalytic sites by an increasing Mg-ATP concentration [Mg-ATP], the ATPase activities of F_1 consist of uni-, bi-, and trisite types. Unisite catalysis is measured at the substoichiometric Mg-ATP concentration ([Mg-ATP] < [F_1]). The unisite activity is very low, and the apparent K_m ATP value is below 20 nM. The apparent K_m ATP values of oligomeric ATPase of $\alpha_3\beta_3$ were about 150 (bisite) and 490μM (trisite). The K_m ATP values of the rotational ATPase of TF_1 (similar to $\alpha_3\beta_3\gamma$) were about 80 (bisite) and 490μM (trisite). Only one mole of [^{3}H]Bz-ADP per $\alpha_3\beta_3$ inhibited its ATPase activity, as both were MF_1 and TF_1 (Aloise *et al*., 1991). This single-hit inactivation and cooperativity are inherent properties of the symmetrical $\alpha_3\beta_3$, but are not due to the interaction with γ.

THE $\alpha_3\beta_3\gamma$ AND ITS HYBRIDS WITH DEFECTIVE α AND β

The major role of γ, a rotating "eccentric cam" in $\alpha_3\beta_3$, is to release Mg-ATP from β_T by changing the conformation (Leslie and Walker, 2000; Oster and Wang, 2000). Because of negative cooperativity between the catalytic sites, the first ATP binds very tightly ($K_d = 10^{-12}$ M), and the last hardly binds at all. Because of this extreme K_d value, ATP is synthesized as F_1-ATP complex without the addition of external energy. In fact, incubating ADP-TF_1 (1:1) complex with P_i and Mg^{2+}, produces TF_1-bound ATP (ATP: ADP: $TF_1 = 0.55{:}0.45{:}1$) (Yohda *et al*., 1986). The addition of γ to $\alpha_3\beta_3$ also changes sensitivity to an inhibitor (Paik *et al*., 1993). Two schemes of hydrolytic cycles have been proposed (Leslie and Walker, 2000). In scheme (a), ATP binding to β_E results in a major conformational change in β_E, which, in turn, rotates γ by $2\pi/3$, and converts β_D to an open conformation. In the alternative scheme (b), ATP binding to β_E promotes ATP hydrolysis at β_D, and the hydrolysis results in a large conformation change in β_D and the release of ADP + P_i. Scheme (a) is more probable, because large conformational change in the isolated β_E was revealed by NMR (Yagi *et al*., 1999). Another new mechanism of ATP hydrolysis via CCC type (full occupancy of three sites) has been proposed (Weber and Senior, 2000). This is based on the nucleotide-dependent fluorescence change of EβY331W without X-ray crystallography. As discussed in the previous section, only modified CCC′ type is compatible with the results on TF_1 (Kagawa, 1999; Tsunoda *et al*., 1999). There should be a transient β_E to allow nucleotide release and binding.

Hybrid $\alpha_3\beta_3\gamma$ Containing 1–3 Subunits with Defective P-Loop

The subunit–subunit interactions via $\alpha\beta$ interfaces were analyzed using homogeneous hybrids of T$\alpha_3\beta_3\gamma$ containing 1, 2, or 3 defective subunits (αi or βi). To isolate T$\alpha_3\beta_3\gamma$ containing 1, 2, or 3 αi or βi, a decaglutamate tag was introduced to αi (Bald *et al*., 1999) or βi (Amano *et al*., 1996) (Fig. 1, bottom, green). After reassembly of the wild type and the mutant into the mixture of four hybrids, they were separated into homogeneous hybrids by ion-exchange chromatography.

The T$\alpha_3\beta_3\gamma$ hybrids with Tβ carrying an inactive catalytic site (βi = TβE190Q tagged with decaglutamate) revealed that normal steady-state ATPase activity, catalytic cooperativity, and unisite ATPase activity require(s) 3, 2, and 1 intact β(s), respectively (Amano *et al*., 1996). In α, TαQQ200 (MαQ208) of the noncatalytic site occupies a position equivalent to that of catalytic TβE190. Thus, α, like the TβE190Q mutation cannot hydrolyze ATP.

The hybrid T$\alpha_3\beta_3\gamma$ containing 1, 2, or 3 defective noncatalytic site(s) in the α subunits (αi) were prepared. To destroy the noncatalytic site of α, the following mutations

were introduced: αi = TαK175A/T176A/D261A/D262A with a decaglutamate tag (Bald *et al*., 1998). The hybrid T$\alpha_3\beta_3\gamma$ displayed a substantial steady-state activity depending on the number of αi (Fig. 2. of ref. Amano *et al*., 1999 with different protein concentrations). The result indicates that one wild-type α is sufficient to maintain the steady-state catalysis and can potentially relieve all three βs from inhibition by Mg-ADP. TαD261N (Yohda *et al*., 1988) failed to dissociate inhibitory Mg-ADP (Jault *et al*., 1995). These results also suggest that the interaction between three noncatalytic sites is not so powerful as that between catalytic sites, which are strictly required for steady-state ATPase. Moreover, TF_o-$(\alpha i)_3\beta_3\gamma$ reconstituted into liposomes can synthesize ATP and is insensitive to azide (Bald *et al*., 1998). Thus, the noncatalytic site is not necessary during ATP synthesis.

INTRAMOLECULAR ROTATION

The single molecule analysis of rotating F_oF_1 (Sambongi *et al*., 1999) is controversial (Tsunoda *et al*., 2000). Thus, we discuss here only the real time imaging of $\alpha_3\beta_3\gamma$ fixed on a bead (Kinoshita, 1999). In the presence of Mg-ATP, the filament attached to γ rotated in a counterclockwise direction ($\beta_D \rightarrow \beta_E \rightarrow \beta_T \rightarrow$) when viewed from the membrane side. The work completed by the rotation is the frictional torque multiplied by the angle of rotation. The hydrodynamic frictional drag coefficient (ξ) of the actin filament for the propeller rotation is given by $\xi = (\pi/3)\eta L^3/[\ln(L/2r)\text{-}0.447]$, where $\eta(10^{-3}\text{Nsm}^{-2})$ is the viscosity of the medium, L the length of the actin filament (1–4 μm), and r (5 nm) the radius of the filament (Yasuda *et al*., 1998). The observed rate of filament rotation rates at 2 mM ATP are 7, 1, and 0.1 rps (revolutions per second), when the lengths of f-actin are 1, 2, and 4 μm, respectively (Yasuda *et al*., 1998). By shortening the f-actin and by extrapolating the external work to zero, the calculated internal friction, if any, was very low. The frictional torque $\xi\omega$ was about 40 pN/nm, where ω is the angular velocity. The stoichiometry of three ATPase catalytic sites per single γ in F_1 indicates a nonload rotary rate of 17 rps as calculated from the ATPase activity of 52 ATP molecules metabolized per second. The ω of γ in the $\alpha_3\beta_3$ decreases at ATP concentrations below 2 μM (Yasuda *et al*., 1998). For short f-actin (0.8–1.2 μm), the rate ω at 20 nM-2 mM ATP fitted simple Michaelis-Menten kinetics [$V_{max}(\omega) = 3.9$ rps, and $K_m(\omega) = 0.8$ μM) (Yasuda *et al*., 1998]. Thus, the rotation may be fueled by individual ATP molecules without requiring the simultaneous consumption of two or more of them. The rotational rate depends on both the frictional load and ATP binding. At higher ATP concentrations (trisite catalysis), the rotational rate was saturated at the level determined by the frictional load.

CROSS LINKING OF SUBUNITS TO FIX THE DOMAIN MOTION

The α–β Cross Linking

Both the catalytic and noncatalytic sites of F_1 were cross linked with 2,8-diN3-ATP (α and β, 9.6 Å apart), to form both $\alpha\beta$ dimers and trimers (Schäfer *et al*., 1995). The adenine-binding pocket cross linked with 2-azido-ATP is TβY341 (=MβY345), and the mutants TβY341A (or C or L) have low activity (Kaibara *et al*., 1996).

The β–β Cross Linking of Closed Form βs

The presence of the two closed β and one open β structure CCO of F_1 in the reaction was confirmed by cross linking two closed β at the position of MβI390 (=TβI394, Fig. 3, I in red circle) of each β (Tsunoda *et al*., 1999). The distance between the nearest α carbon atoms of the MβI390 in Mβ_D and Mβ_T was only 0.79 nm, while those between Mβ_E and Mβ_D and Mβ_E and Mβ_T were 2.58 and 2.40 nm, respectively. The distance between TβI386 of Tβ_E in $\alpha_3\beta_3$ is 3.27 nm (Shirakihara *et al*., 1997). Thus, the β-β cross link could form in the CCO, but not in COO and OOO types of TF_1. The mutant TβI386C was assembled into the Tα_3(TβI386C)$_3\gamma$ subcomplex. Tβ_T and Tβ_D were cross-linked via a disulfide bond between the two TβI386C by oxidation in the presence of Mg-AT(D)P (Tsunoda *et al*., 1999). The β-β cross-linked Tα_3Tβ(TβI386C)$_2\gamma$ was inactive, but was reactivated by reduction with dithiothreitol. The CCC-type MF_1 (Bianchet *et al*., 1998) is impossible because of steric collision.

At the entrance to the crevice of the P-loop, the distances between MβD315 (=TβD311, in VIII) and MβR337 (=TβR333 in IX) are 0.30, 0.37, and 1.03 nm in Mβ_T, Mβ_D, and Mβ_E, respectively (Fig. 3, D and R in green circle). Cross linking of TβD311C and TβR333C fix β in the closed form in which α–helix C and α-helix B become parallel (Ren *et al*., 1999). In the reassembled α_3(βD311C/R333C)$_3\gamma$, less than two βD311C/R333Cs were cross linked in the presence of Mg–nucleotide, thus, the CCO or COO types can arise. However, under high nucleotide conditions, all βs bind the ligand (Weber and Senior, 2000), and an approximate threefold symmetry has been detected in rat liver MF_1 (Bianchet *et al*., 1998). As

will be discussed below, the βDELSEED region is elastic (Kagawa, 1999), and C′CC form may arise, in which C′ is deformed C.

The β–γ Cross Linking

Since γ is the rotational axis, any cross linking between γ and $\alpha_3\beta_3$ results in a loss of multisite catalysis, but unisite catalysis remains in the $\beta\gamma$ cross-linked EF_1 (Garcia and Capaldi, 1998). Three points of contact between Mγ and Mβ are catalytic VII and VIII (D316, T318, and D318), and noncatalytic IX. These areas of α/β interfaces, are directly deformed by γ during rotation. In β_T, the noncatalytic IX is the closest to γRGL (γ3 in Fig. 3), which is 2 nm from the central axis may transfer torque to DELSEED. The conserved MγQ255 (=EγQ269) may also transfer torque via MβD316 and MβD318 in VIII (γ2 in Fig. 3) (Omote *et al.*, 1998). The interaction between γ1 and VII is not established.

THE HINGE OF DOMAIN MOTIONS

F_1 is a flexible entity (Hayward, 1999; Yan *et al.*, 1999), and it is necessary to detect the hinge point between open and closed β that may generate the torque of γ rotation (Oster and Wang, 2000; Kagawa, 1999). We cannot estimate elasticity solely on the physical property of the separate α-helix and β sheet. These structures are mechanically grouped in a protein. For example, in βT, α-helix G, β sheets 7, 3, and 8, and α-helix B are packed in parallel, but in β_E, the distances between the helix–sheets–helix, especially that between β sheet 7 and 3, are widened. Thus, hinge of the domain is important to estimate elasticity. An angle formed by four consecutive Cα atoms in polypeptide backbones was computed from X-ray crystallography of the proteins. The difference in this angle from the equivalent residues between the open and closed forms was used to detect the pivot (Yan *et al.*, 1999). The pivot residues of Tβ that change the ϕ and ψ angles of a Ramachandran plot by more than $5\pi/9$ on addition of AT(D)P are V162, G163, H179, G180, and G181 (Abrahams *et al.*, 1994). V162 and G163 belong to the P-loop (ATP-binding site) at IV. H179, G180, and G181 are located at the loop between the loop B-4 located at the outer end of β(Shirakihara *et al.*, 1997) (Fig. 3, H,G,G in yellow circle). The open–close angle between MβDELSEED (or TβDELSDED) and VIII of the catalytic interface (loop 7G) is about $\pi/6$. The loop B-4 connects the P-loop and the GER loop near V in the catalytic interface (Fig. 2). The residues (TβG180, TβE361, TβS30, and TβH179) in the rotation also show large changes in the ϕ and ψ angles (Masaike *et al.*, 2000). The simultaneous mutagenesis of TβH179A, TβG180A, and TβG181A caused almost a complete loss (99%) of ATPase activity. The steady-state ATPase activities of α_3(mutant $\beta)_3\gamma$ were 65, 23, 4.3, and 160 s^{-1} in wild-type Tβ, TβH179A, TβG180A, and TβG181A, respectively. However, TβG180A enhanced and TβG181A abolished the propensity to generate the kinetically trapped Mg-ATP inhibited form (Masaike *et al.*, 2000). Despite the hindrance to the formation of Tβ_E in the α_3(mutant $\beta)_3\gamma$ thus generated, the mean rotational torque was not changed (Masaike *et al.*, 2000). Although, other causes may explain the loss of ATPase activity with normal torque in the hinge muntant, the rotational velocity of the mutants is only 0.2 to 5 (0.6 to 15 ATP/sec) compared with 4.3 to 160 ATP/sec hydrolyzed (turnover rate) in free $\alpha\beta\gamma$. Thus, only a few hits of ATP at the catalytic site are required to drive rotation, even when ATPase levels are dramatically decreased.

ELASTIC ENERGY STORED DURING THE τ_{step}

The time per $2\pi/3$ revolution (τ_{120}) is composed of the cycle time for unloaded ATPase, (τ_{ATP}) and $\tau_{step} = (2\pi/3)\xi/N$), thus, $\tau_{120} = \tau_{ATP} + \tau_{step}$. The τ_{step} is prolonged by the load of friction required to rotate the f-actin (Yasuda *et al.*, 1998). The rotational rate at 2 mM ATP is 0.1 rps, when the length of f-actin is 4 μm (K_m ATP = 0.8 μM; Yasuda *et al.*, 1998). After the binding of ATP to Tβ in a very short time (τ_{ATP}), the chemical energy of ATP hydrolysis should be stored in the $\alpha_3\beta_3\gamma$-actin complex during τ_{step} (about 3 sec), perhaps as an elastic energy. The maximum energy stored during a $2\pi/3$ rotation is approximately 80 pN/nm, a value close to the free energy of ATP hydrolysis. The actin filament bends very little during the load (see photographs in Noji *et al.*, 1997), and thus the energy is stored in $\alpha_3\beta_3\gamma$. When the elastic energy exceeds a certain threshold value, one ATP molecule bound at the P-loop around IV is released.

Any force applied to a subunit is transferred to the next one only through the contact area (Fig. 2 and Table I). Of course, the stress–strain relations should be calculated by the stress tensor, but the structure of $\alpha_3\beta_3\gamma$ is too complicated to apply the tensor. Thus, more simplified scheme of elastic energy transmission was proposed (Oster and Wang, 2000; Cherepanov *et al.*, 1999).

To estimate the elastic energy in $\alpha_3\beta_3\gamma$ under torque, both Poisson ratio (σ) and the Young's modulus (E, the dimension is $Pa = N/m^2$), of the protein are needed. The torsional strain energy is $U = \pi R^4 E\theta^2/8L(1+\sigma)$, where θ is the torsional angle, L is the length of γ, and R is the

radius of γ. The modulus of elasticity (k) of many proteins reported by Gekko's group (Kamiyama and Gekko, 2000), will be useful to estimate E using the equation: $E = 3k$ (1-2σ). The Poisson ratio of about 0.4 for proteins is acceptable because wide varieties of proteinlike substances, such as rubber (0.46–0.49) and polystylene (0.34), (Rikanenpyou, Maruzen, Tokyo, 1973) show similar values. The ligands induce a large change in the elasticity of protein as shown by Gekko's group (Kamiyama and Gekko, 2000). Junge's group adopted E of actin (1.8×10^9 N/m^2) (Yanagida *et al*., 2000), but E of a collagen triple helix (5×10^9 N/m^2) (Hoffmann *et al*., 1984) is better, because of the interaction between the α-helices in F_1 (personal communication, T. Yanagida, 2000). Since the tortional strain energy is proportional to E, the estimated value of U is about 2.8-fold of that reported by Junge's group (50 kJ per $2\pi/3$ rotation) (Fig. 1 of Cherepanov *et al*., 1999).

However, if $\alpha_3\beta_3\gamma$ is subjected to an external torque of 42 pN/nm, the average force acting on the α/β interfaces of about 2 nm from the γ-axis will be 21 pN. The torque of γ is applied through three points of γ (Fig. 3, blue circles, γ 1–3), mainly to β_E at γ2 and to β_T at γ3 (Abrahams et al., 1994). The torsional strain applied at γ2 to VIII and transferred to III–VII, but not to I, I′, and II, which are immobile and connected to III via a slender main chain (Fig. 3, red*). The strain applied at γ3 (the most eccentric portion of Mγ RGL sequence) to the DELSE(D)ED sequence (Fig. 3) of β_T is propagated from IX–XI to IV, which moves DELSE(D)ED away from γ, and the hinge is open. The elasticity of DELSEED was demonstrated by the fact that any of the residues EβD390, EβD391, and EβS393 in that sequence, can be cross linked to the same residue in the γ subunit (Kagawa, 1999, references therein). Thus, the elastic conformational change at P-loop will release ATP (Oster and Wang, 2000; Kagawa, 1999). Elasticity around the P-loop was shown by cross linking the $\alpha\beta$ interface with a very short diazidonucleotide (Schäfer *et al*., 1995). The binding of Mg-ATP to Mβ_E at K162, K163, E192, E199, and D256 around the P- and GER-loops bring βR260 of Mβ_T close to αF299 and αS344 of Mα. This conformational signal is transferred through H bonds between Y300, R304, and Y244 of Mα (Ren and Allison, 2000). However, correlating these residue interactions with local elastic energy is difficult.

Elastic energy may be stable at least for a few seconds of τ_{step}. The length of τ_{step} can be extended if the proton-driven rotation is stopped by removing ADP + P_i (so-called state 4 respiration). Because of uncoupling (by uncoupling proteins etc.), decoupling, and noncoupling, estimating the stability of elastic energy is difficult in the mitochondrial membrane (Kagawa *et al*., 1999). Dissociation of $\alpha_3\beta_3$ into $\alpha_1\beta_1$ by the ATPase reaction has been analyzed using a synchrotron (Sato *et al*., 1995), and the time course of dissociation was in the same range as the rotation of $\alpha_3\beta_3\gamma$.The elastic energy stored during the domain motions in protein has been discussed in detail (Hayward, 1999).

CONCLUSION

X-ray crystallography of MF_1 and T$\alpha_3\beta_3$, together with domain cross-linking revealed the domain motions that release ATP-Mg from β_T. The α/β interfaces of β constitute the pathway of signal and energy in F_1 (Table I and Fig. 2). ATP synthesis/hydrolysis is dependent on the $\alpha\beta$ interaction at catalytic III to VIII in β_E, and I, I′, and II fix the barrel domains for the stator (Fig. 3). Rotation of γ in $\alpha_3\beta_3$ with torque of 42 pN/nm applies pressure on catalytic β_E at γ2 and at β_T, at γ3, etc., cause the hinge motions at H179, G180, and G181, and then at V162 and G163 at IV of the P-loop of Tβ (Masaike *et al*., 2000). During the rotation, the contact areas are increased from 7 (93 atoms in Mβ_E) to 11 (176 atoms in MβD) (catalytic IV, IX, X, and XI, and noncatalytic VIII and IX) (Table I). If the entrance of the P-loop is cross linked, the activity is lost because hinge motion is lost (Ren *et al*., 1999). The strain is distributed at the α/β interfaces including IV, V, and VIII near the P-loop, GER-loop, and switch domain, respectively, of β. This brings βR260 of MβT close to αF299 and αS344 of Mα and the conformational signal is transferred through H-bonds in Mα.

The models of elastic energy in F_oF_1 (Oster and Wang, 2000; Cherepanov *et al*., 1999) are still contradictory to the experimental results and are not related to the actual domain movements in F_1. The following experimental results are important.

1. Single-stalk F_oF_1 (Fig. 1 right). X-ray crystallography (Stock *et al*., 1999) and electron microscopy (Kagawa and Racker, 1966b) of some F_oF_1 preparation show only one stalk. The rotation of F_o-*c* observed (Sambongi *et al*., 1999) may be caused by loss of the stator (Tsunoda *et al*., 2000). X-ray crystallography indicates that number of the *c* subunits is 10 (Stock *et al*., 1999). Thus, F_o is rotated by the $\pi/5$ step, not the $2\pi/3$, if the stator is intact (double stalk F_oF_1). Then, the stoichiometry cannot be an integer but the transient elastic energy will explain the high efficiency of rotation.

2. The open–close motion is the inherent property of the isolated Tβ (Fig. 1, left). X-ray crystallography, IR, and NMR of isolated β revealed that it is in the open form (O), which is converted into the closed form (C) by adding Mg-ATP. This O–C conversion is independent of

interactions with other subunits. The conversion depends on the pivot residues (H179, G180, and G181) (Fig. 3, right). This motion is transferred through α/β interfaces and the elastic rotates γ.

3. CCO and CCC type of F_1. The CCO type of F_1, shown by X-ray crystallography (Abrahams *et al*., 1994), has been graphically rotated in the calculation of elastic energy. However, ATPase was not active in the conditions for the CCO-type crystal. On the other hand, the CCC-type F_1 (Bianchet *et al*., 1998; Weber and Senior, 2000) is incompatible with the results of cross linking β–β (Tsunoda *et al*., 1999), and TβD311-R333 (Ren *et al*., 1999). Thus, it should include the elastically deformed C (C′).

4. Bi- or trisite catalysis in rotation of $\alpha_3\beta_3\gamma$. The unisite reaction conditions at 1 mM ATP is the base of calculation (Oster and Weber, 2000), but unisite catalysis is observed below nanomolar range, and the $2\pi/3$ step rotation of $\alpha_3\beta_3\gamma$ is observed at higher ATP concentrations: about 150 (bisite) and 490 μM (trisite).

5. H-bonds in ATP binding. The "binding-zipper" is based on the thermal zippering of H bonds between Mg-ATP and P-loop. There are electrostatic force between the negative charges of phosphate and the surrounding guanidium and ammonium. Tritium exchange could not show zipping of H bonds (Noji *et al*., 1996). The electrostatic energy between residues is several hundredfold larger (Hall and Pavitt, 1984) and long reaching than that in H bond (0.3 nm, directional) and hydrophobic interaction (very near). Electrostatic force between residues (Table I, red and blue letters) is important in elastic displacement during the rotation.

6. Hardness of the structure. TF_1 is harder than mesophilic F_1s, but this stability is mainly limited to the immobile domains I, I′, and II. The relevant residues in III–XI and the hinge accepting the elastic strain are conserved among F_1s.

Finally, these residue movements are not yet expressed by the stress tensor inside $\alpha_3\beta_3\gamma$. X-ray crystallography has been regarded as a purely static technique, and models of elastic energy in F_oF_1 discussed here are necessarily speculative. However, time-resolved crystallography (Moffat, 1998) of F_1 during the photolysis of caged ATP will overcome the limitations of the present X-ray data to analyze the domain motions.

ACKNOWLEDGMENTS

We thank Dr. Y. Shirakihara of the National Institute of Genetics for calculating the residue pairs within 0.40 nm across the catalytic and noncatalytic interfaces of the α and β subunits of TF_1 and MFM_1. Thanks are due to Prof. K. Miki of Kyoto University for providing unpublished data about the Tβ monomer. We also thank Prof. M. Yoshida at Tokyo Institute of Technology, Prof. M. Futai at Osaka University, Prof. H. Kihara of Kansai Medical University, and Dr. E. Muneyuki at Tokyo Institute of Technology for discussing their studies of TF_1. This work was supported by Grants in Aid for High Technology Research Center from the Ministry of Education, Science and Culture of Japan.

REFERENCES

Abrahams, J. P., Leslie, A. G. W., Lutter, R. and Walker, J. E. (1994). *Nature(London)***370**, 621–628.
Aloise, P., Kagawa, Y., and Coleman, P. S. (1991). *J. Biol. Chem*. **266**, 10368–10376.
Amano, T., Hisabori,T., Muneyuki, E., and Yoshida, M. (1996). *J. Biol. Chem*. **271**, 18127–18133.
Amano, T., Matsui, T., Muneyuki, E., Noji, H., Hara, K., Yoshida, M., and Hisabori, T. (1999). *Biochem. J*. **343**, 135–138.
Arai, M., and Kuwajima, K. (2000). *Advan. Protein Chem*. **53**, 209–282.
Argos, P., Rossmann, M. G., Grqu, U. M., Zuber, H., Frank, G., and Tratschin, J. D. (1979). *Biochemistry* **18**, 5698–5703.
Bald, D., Amano, T., Muneyuki, E., Pitard, B., Rigaud, J-L., Kruip, J., Hisabori, T., Yoshida, M., and Shibata, M. (1998). *J. Biol. Chem*. **273**, 865–870.
Bianchet, M. A., Hullihen, J., Pedersen, P. L., and Amzel, L. M. (1998). *Proc. Natl. Acad. Sci. USA* **95**, 11065–11070.
Boyer, P. D. (1997) *Annu. Rev. Biochem*. **66**, 717–749.
Burgard, S., Nett, J. H., Sauer, H. E., Kagawa, Y., Schäfer, H-J., Wise, J. G.,Vogel, P. D., and Trommer, W. E. (1994). *J. Biol. Chem*. **269**, 17815–17819.
Cherepanov, D. A., Mulkidjanian, A. Y., and Junge, W. (1999). *FEBS Lett*. **449**, 1–6.
Collinson, I. R., Skehel, J. M., Fearnley, I. M., Runswick, J. M., and Walker, J. E. (1996). *Biochemistry* **35**, 12640–12646.
Futai, M., and Omote, H. (1996). *J. Bioenerg. Biomembr*. **28**, 409–414.
Futai, M., Noumi, T., and Maeda, M. (1989). *Annu. Rev. Biochem.* **58**, 111–136.
Garcia, J. J., and Capaldi, R. A. (1998). *J. Biol. Chem*. **273**, 15940–15945.
Hall, D., and Pravitt, N. (1984). *Compt. Chem*. **5**, 441–450.
Hayward, S. (1999). *Proteins* **36**, 425–435.
Hirata, H., Ohno, K., Sone, N., Kagawa, Y., and Hamamoto, T. (1986). *J. Biol.Chem*. **261**, 8939–8943.
Hofmann, H., Voss, T., Kuhn, K., and Engel, J. (1984). *J. Mol. Biol*. **172**, 325–343.
Ichida, M., Hakamata, Y., Hayakawa, H., Ueno, E., Ikeda, U., Shimada, K., Hamamoto, T., Kagawa, Y., and Endo, H. (2000). *J. Biol. Chem*. **275**, 15992–16001.
Jaenicke, R., and Boehm, G. (1998). *Curr. Opinion Struct. Biol*. **8**, 738–748.
Jault, J. M., Matsui, T., Jault, F. M., Kaibara, C., Muneyuki, E., Yoshida, M., Kagawa, Y., and Allison, W. S. (1995). *Biochemistry* **34**, 16412–16418.
Jones, P. C., Jiang, W., and Fillingame, R. H. (1998). *J. Biol. Chem*. **273**, 17178–17185.
Kagawa, Y. (1999). *Advan. Biophys*. **36**, 1–25.
Kagawa, Y., and Hamamoto, T. (1996). *J. Bioenerg. Biomembr*. **28**, 421–431.
Kagawa, Y., and Hamamoto, T. (1997). *Biochem. Biophys. Res. Commun*. **240**, 247–256.
Kagawa, Y., and Racker, E. (1966a). *J. Biol. Chem*. **241**, 2467–2474.

Kagawa, Y., and Racker, E. (1966b). *J. Biol. Chem*. **241**, 2475–2482.
Kagawa, Y., and Racker, E. (1971). *J. Biol. Chem*. **246**, 5477–5487.
Kagawa, Y., Ishizuka, M., Saishu, T., and Nakao, S. (1986). *J. Biochem*. **100**, 923–934.
Kagawa, Y., Ohta, S., Harada, M., Sato, M., and Ito, Y. (1992). *Ann. N.Y. Acad. Sci*. **671**, 366–376.
Kagawa, Y., Hamamoto, T., Endo, H., Ichida, M., Shibui, H., and Hayakawa, M. (1997). *Biosci. Rept*. **17**, 115–146.
Kagawa, Y., Cha, S-H., Hasegawa, K., Hamamoto, T., and Endo, H. (1999). *Biochem.Biophys. Res. Commun*. **266**, 662–667.
Kaibara, C., Matsui, T., Hisabori, T., and Yoshida, M. (1996). *J. Biol. Chem*. **271**, 2433–2438.
Kamiyama, T., and Gekko, K. (2000). *Biochim. Biophys. Acta* **1478**, 257–266.
Kinoshita, K. Jr. (1999). *FASEB J. Suppl*. **2**, S201–S208.
Masaike, T., Mitome, N., Noji, H., Muneyuki, E., Yasuda, R., Kinoshita, K., Jr., and Yoshida, M. (2000). *J. Exp. Biol*. **203**, 1–8.
Le, N. P., Omote, H., Wada, Y., Al-Shawi, M. K., Nakamoto, R. K., and Futai, M. (2000). *Biochemistry* **39**, 2778–2783.
Leslie, A. G. W., and Walker, J. E. (2000). *Phil. Trans. R. Soc. Lond. B* **355**, 465–472.
Mitchell, P. (1979) *Science* **206**, 1148–1159.
Moffat, K. (1998). *Acta Crystallogr. A*. **54**, 833–841.
Noji, H., Amano, T., and Yoshida, M. (1996). *J. Bioenerg. Biomembr*. **28**, 451–457.
Noji, H., Yasuda, R., Yoshida, M., and Kinosita, K. Jr. (1997). *Nature (London)* **386**, 299–302.
Ohta, S., and Kagawa, Y. (1986). *J. Biochem*. **99**, 135–141.
Ohta, S., Tsuboi, M., Yoshida, M., and Kagawa, Y. (1980). *Biochemistry* **19**, 2160–2168.
Omote, H., Nga, P. L., Park, M-Y., Maeda, M., and Futai, M. (1995). *J. Biol. Chem*. **270**, 25656–25660.
Omote, H., Tainaka, K., Fujie, K., Iwamoto-Kihara, A., Wada, Y., and Futai, M. (1998). *Arch. Biochem. Biophys*. **358**, 277–282.
Oster, G., and Wang, H. (2000). *Biochim. Biophys. Acta* **1458**, 482–510.
Paik, S. R., Yokoyama, K., Yoshida, M., Ohta, T., Kagawa, Y., and Allison, W. S. (1993). *J. Bioenerg. Biomembr*. **25**, 679–684.
Pedersen, P. L. (1996). *J. Bioenerg. Biomembr*. **28**, 389–395.
Ren, H., and Allison, W. S. (2000). *J. Biol. Chem*. **275**, 10057–10063.
Ren, H., Dou, C., Stelzer, M. S., and Allison, W. S. (1999). *J. Biol. Chem*. **274**, 31366–31372.
Saika, K., and Yoshida, M. (1995). *FEBS Lett*. **368**, 207–210.
Saika, K., Inaka, K., Matsui, T., Yoshida, M., and Miki, K. (1994). *J. Mol. Biol*. **242**, 709–711.
Sambongi, Y., Iko, Y., Tanabe, M., Omote, H., Iwamoto-Kihara, A., Ueda, I.,Yanagida, T., Wada, Y., and Futai, M. (1999). *Science* **286**, 1687–1688.
Sasaki, N., Shimada, T., and Sutoh, K. (1998). *J. Biol. Chem*. **273**, 20334–20340.
Sato, M., Ito, Y., Harada, M., Kihara, H., Tsuruta, H. S., Ohta, S.,and Kagawa, Y. (1995). *J. Biochem*. **117**, 113–119.
Schäfer, H-J., Rathgeber, G., and Kagawa, Y. (1995). *FEBS Lett*. **377**, 408–412.
Senter, P., Eckstein, F., and Kagawa, Y. (1983). *Biochemistry* **22**, 5514–5518.
Shibui, H., Hamamoto, T., Yohda, M., and Kagawa, Y. (1997). *Biochem. Biophys. Res. Commun*. **234**, 341–345.
Shirakihara, Y., Leslie, A. G. W., Abrahams, J. P., Walker, J. E., Ueda, T., Sekimoto, Y., Kambara, M., Saika, K., Kagawa, Y., and Yoshida, M. (1997). *Structure*. **5**, 825–836.
Stock, D., Leslie, A. G. W., and Walker, J. E. (1999). *Science* **286**, 1700–1705.
Tozawa, K., Sekino, N., Soga, M., Yagi, H., Yoshida, M., and Akutsu, H. (1995). *FEBS Lett*. **376**, 190–194.
Tsunoda, S. P., Aggeler, R., Noji, H., Kinoshita, K., Jr., Yoshida, M., and Capaldi,R. A. (2000). *FEBS Lett*. **470**, 244–248.
Tsunoda, S. P., Muneyuki, E., Amano, T., Yoshida, M., and Noji, H. (1999). *J. Biol. Chem*. **274**, 5701–5706.
Wang, Z. G., and Ackerman, S. H. (2000). *J. Biol. Chem*. **275**, 5767–5772.
Weber, J., and Senior, A. E. (2000). *Biochim. Biophys. Acta* **1458**, 300–309.
Wilkens, S., and Capaldi, R. A. (1998). *Biochim. Biophys. Acta* **1365**, 93–97.
Xu, T., Zanotti, F., Gaballo, A., Raho, G., and Papa, S. (2000). *Eur. J. Biochem*. **267**, 4445–4455.
Yagi, H., Tozawa, K., Sekino, N., Iwabuchi, T., Yoshida, M., and Akutsu, H. (1999). *Biophys. J*. **77**, 2175–2183.
Yan, B., Zhang, W., Ding, J., and Arnold, E. (1999). *J. Protein Chem*. **18**, 807–811.
Yanagida, T., Kinanuma, K., Tanaka, H., Hikikoshi-Iwane, A., and Esaki, S. (2000). *Curr. Opinion Cell Biol*. **12**, 20–25.
Yasuda, R., Noji, H., Kinoshita, K. Jr., and Yoshida, M. (1998). *Cell* **93**, 1117–1124.
Yohda, M., Kagawa, Y., and Yoshida, M. (1986). *Biochim. Biophys. Acta* **850**, 429–435.
Yohda, M., Ohta, S., Hisabori, T., and Kagawa, Y. (1988). *Biochim. Biophys. Acta* **933**, 156–164.
Yoshida, M., Sone, N., Hirata, H., and Kagawa, Y. (1975). *J. Biol. Chem*. **250**, 7910–7915.
Yoshida, M., Sone, N., Hirata, H., Kagawa, Y., and Ui, N. (1979). *J. Biol. Chem*. **254**, 9525–9533.
Yoshida, T., Yohda, M., Iida, T., Maruyama, T., Taguchi, H., Yazaki, K., Ohta, T., Okada, M., Endo, I., and Kagawa, Y. (1997). *J. Mol. Biol*. **273**, 635–645.